Using a Patterned Sapphire Template And The Lift-off Technique To Synthesize ZnO Nanoflower Arrays With Enhanced Photoluminescence Properties

Hsien-Wei TSENG
Yango University
Ching-Shan WANG
National Chung Hsing University
Fang-Hsing WANG
National Chung Hsing University
Han-Wen LIU
National Chung Hsing University
Cheng-Fu YANG (cfyang@nuk.edu.tw)
National University of Kaohsiung

Research Article

Keywords: patterned sapphire substrate, template, lift-off, ZnO nanoflower arrays

Posted Date: September 15th, 2021

DOI: https://doi.org/10.21203/rs.3.rs-861281/v1

Abstract

In this study, the hydrothermal method was used to synthesize ZnO nanorods and ZnO nanoflower arrays. Two different substrates were used to prepare the ZnO seed layer. For the p-type silicon <100> wafer, a prepared ZnO gel was deposited as the seed layer using the spin coating method. When a patterned sapphire recess-type substrate was used as a template, Al film, with a thickness of 120 nm, and OE-6370HF AB glue were used as a sacrificial layer and an imprinting lithography carrier for the ZnO seed layer, respectively. To prepare the array-patterned ZnO seed layers with a protrusion structure, a lift-off technique was used. A 0.2 M solution of zinc acetate dihydrate ($Zn(CH_3COO)_2$-$2H_2O$) was used at a synthesis temperature of 90°C and a synthesis time of 10–60 min. Because the ZnO seed layer had a protrusion and matrix structure, the ZnO nanorods grew in the vertical bottom direction to form ZnO nanoflower arrays. X-ray diffraction patterns, scanning electron microscopy, and a focused ion beam system were used to analyze and compare the crystal characteristics and the heights and widths of the ZnO nanorods and ZnO nanoflower arrays. We found that the photoluminescence properties were enhanced in the ZnO nanoflower arrays compared with the ZnO nanorods.

Introduction

Group II–VI metal oxide semiconductors, which include zinc oxide (ZnO), can be used in a wide range of devices. In 1968, researchers grew ZnO single crystals and proved that ZnO had excellent piezoelectric characteristics [1]. At room temperature, ZnO-based materials have a wide direct band gap of about 3.37 eV and a large exciton binding energy of about 60 meV. These materials also have high chemical and thermal stability, a low dielectric constant, high photocatalytic properties, and high transparency in the visible light and infrared ranges. Because ZnO-based films have many superior properties, various methods to deposit ZnO-based films, including the chemical vapor transport method, spray pyrolysis method, metal organic chemical vapor deposition method, pulsed laser deposition method, and sol–gel method, have been investigated. The sputtering method of film deposition is most widely used because it can deposit ZnO-based films with different dopants by the changes in the composition of the prepared targets [2]. ZnO-based films can be used in many different applications, including varistors [3], light emitting diodes [4], optical waveguide and photodetector arrays [5], transparent electrodes [6], dye-sensitized solar cells [7], and sensors for the detection of different objects [8, 9].

Many process technologies have been investigated to fabricate ZnO-based nanomaterials with various crystal shapes. For example, Karthik et al. utilized homogenous precipitation methods with urea and ammonium hydroxide as precipitation agents to synthesize ZnO with structural disarray in the lattice and needle-like microstructures [10]. Zhang et al. utilized $Zn(NH_3)_4^{2+}$ and $Zn(OH)_4^{2-}$ precursors in various solvents under different reaction conditions to synthesize ZnO with various morphologies, including flower-like, prism-like, prickly sphere-like, and rod-like shapes [11]. Chen et al. used the hydrothermal method to synthesize ZnO nanorods (or nanowires), and found that the deposition time and the face direction of the substrates in the hydrothermal bottle were important factors that affected the

morphologies of the ZnO nanomaterials [12]. The researchers also found that the ZnO nanostructures had three different morphologies: beautiful chrysanthemum-like nanoflowers, nanorods, and irregular-plate structure films.

Zhang et al. used a capping-molecule-assisted hydrothermal process to investigate ZnO microcrystals [13]. They found that the synthesized formations of dumbbell-like, disk-like, and flower-like shapes of the ZnO microcrystals depended on the capping molecules that were used. Wang et al. also used the hydrothermal method to synthesize ZnO microcrystals [14]. They found that controlling the pH of the solution, the reaction time, and the concentration of the precursor affected the flower-like rod aggregation, hexagonal pyramid-like rod, and microrod appearances of the ZnO nanomaterials. The hydrothermal method is the most economical, simple, and commonly used method to synthesize ZnO nanostructures.

ZnO nanorods and ZnO nanoflower arrays may have applications in various optoelectronic devices and, thus, it is important to develop methods to synthesize ZnO in these configuration. In this study, we used the hydrothermal method to synthesize ZnO nanorods and ZnO nanoflower arrays using ZnO seed layers on different substrates. In general, ZnO nanorods that are synthesized on a plane-typed substrate perpendicular to the substrate. When ZnO nanorods are used as sensors for different signals, the first sites for contact and reaction are at the top surfaces of the nanorods. When ZnO nanorods are grown in a structure of radiating needles, they can synthesize to form ZnO nanoflowers. When ZnO nanoflowers are used as gas or optical sensors, they have a greater area for contact and reaction sites and then to enhance the reaction sensitivity and the response speed.

The important novel innovation of this study was the development of a low-cost technology to fabricate a patterned ZnO seed layer. This technology involved the use of patterned sapphire templates and the lift-off technique to synthesize ZnO nanoflower arrays. We used synthesis time to analyze the properties of ZnO nanorods synthesized on a p-type silicon (Si) < 100 > wafer, as well as the properties of ZnO nanoflower arrays synthesized on a prepared patterned substrate. The investigated ZnO nanoflowers had different shapes from most reported ZnO nanoflowers, which typically present with prickly sphere-like, rod-like [11], or sea anemone-like morphologies [15]. A series of experiments were performed to investigate the effect of synthesis time on the physical properties, which included the crystal characteristics, morphology, height (or length), diameter, and aspect ratio, and the optical properties, such as the photoluminescence (PL) spectra of the ZnO nanorods and ZnO nanoflower arrays. During the experiments, the synthesis time was varied, but the other parameters were kept constant. The novel analysis of this study was that we investigated and compared the height/diameter (H/D) ratio of the ZnO nanorods and ZnO nanoflower arrays with the PL properties. We proved that for the same synthesis time, the PL emission intensities of the ZnO nanoflower arrays were enhanced compared with the intensities of the ZnO nanorods.

Experimental Procedures

2.1. Preparation of ZnO gel

We used zinc acetate dihydrate ($Zn(CH_3COO)_2$-$2H_2O$), 2-aminoethanol (monoethanolamine) (C_2H_7NO), and ethylene glycol monomethyl ether ($CH_3OCH_2CH_2OH$) to prepare a solution of 0.75 M Zn^+ ions. The solution was heated to 60°C, stirred for 2 h, and left for 48 h. Figure 1(a) shows the transparent ZnO gel solution that was obtained.

2.2. Process of synthesis ZnO nanorods

To prepare the Al sacrificial layer, a 2-inch sapphire substrate, provided by Shun Haw Technology Ltd., Taiwan, was used. A schematic diagram and a cross-sectional view of the substrate is shown in Figs. 2(a) and 2(b), respectively. The average bottom width and average height of the substrate were 0.37 μm and 0.48 μm, respectively. First, we used the evaporation method to deposit the Al sacrificial layer on the sapphire substrate at a thickness of approximately 120 nm. The sapphire substrates were then put into a tube furnace and heated to 500°C for annealing. The annealing time was 1 h and the pressure in the furnace was controlled at 1.2 bar; a mixing gas of 90% Ar + 10% H_2 was introduced during the annealing process.

2.3. Preparation of the Al sacrificial layer

To prepare the Al sacrificial layer, a 2-inch sapphire substrate, provided by Shun Haw Technology Ltd., Taiwan, was used. A schematic diagram and a cross-sectional view of the substrate is shown in Figs. 1(a) and (b), respectively. The average bottom width and average height of the substrate were 0.37 μm and 0.48 μm, respectively. First, we used the evaporation method to deposit the Al sacrificial layer on the sapphire substrate at a thickness of approximately 120 nm. The sapphire substrates were then put into a tube furnace and heated to 500°C for annealing. The annealing time was 1 h and the pressure in the furnace was controlled at 1.2 bar; a mixing gas of 90% Ar + 10% H_2 was introduced during the annealing process.

2.4. Preparation of ZnO-seed layer using spin coating method

The ZnO gel was applied to fully cover the surface of the patterned sapphire template with the Al sacrificial layer. The spinning speed and time were set to 2,000 rpm and 30 s, respectively. After the coating process, the ZnO gel-coated template was baked at 300°C for 10 min to dry and harden the coating film and to volatilize and remove the organic solvent. The processes of spin coating and baking were repeated six times, after which a ZnO thin layer, or seed layer, was obtained, as shown in Fig. 1(c).

2.5. Processes of synthesis ZnO nanoflower arrays

Before the ZnO thin layer was lifted off, it was coated with optical OE-6370HF AB glue to act as a carrier, as shown in Fig. 1(d). We then used lift-off technology and imprint lithography the to make patterns on the ZnO thin layer to create the ZnO seed layer A solution of $K_3Fe(CN)_6$:KOH:H_2O (10 g:1 g:100 ml) was used to etch the Al sacrificial layer. The protrusion and patterned ZnO seed layer was then obtained, as shown in Figs. 1(e) and 1(f). Next, the ZnO seed layer was attached to the p-type Si < 100 > substrate

using OE-6370HF AB glue, as shown in Fig. 1(g). Finally, a 0.2-M solution of zinc acetate dihydrate ($Zn(CH_3COO)_2$-$2H_2O$ was used to synthesize the ZnO nanoflower arrays at a syntesis temperature of 90°C and at synthesis times of 10 min, 20 min, 30 min, and 60 min (Fig. 1(h). After the ZnO nanorods and ZnO nanoflower arrays were synthesized, an X-ray diffractometer (XRD) was used to analyze their crystalline phases. A field emission scanning electron microscope (FESEM) was used to observe the surface morphologies of the ZnO nanorods and ZnO nanoflower arrays. A focused ion beam (FIB) system was used to cut the ZnO nanorods, the prepared patterned ZnO seed layer, and the ZnO nanoflower arrays to observe their cross-sectional morphologies. The PL emission properties of the ZnO nanorods and ZnO nanoflower arrays were measured in the wavelength range of 350 ~ 650 nm at room temperature using a Horiba Jobin Yvon iHR550 fluorescence spectrophotometer. A single wavelength laser at a wavelength of 325 nm was used as the excitation light source.

Results And Discussion

The diffraction peaks of the ZnO seed layer located at the 2θ values of 31.9°, 34.6°, 36.48°, 47.64°, and 56.78° corresponded to the diffraction peaks at the (100), (002), (101), (102), and (110) planes, respectively, as shown in Fig. 3. Compared with the Joint Committee on Powder Diffraction Standards (JCPDS) card No. 36-1451, we found that the ZnO seed layer presented with a wurtzite structure that had a structure of hexagonal close-packed structure (HCP). The highest diffraction peak was located at the 2θ value of 34.6°, which corresponded to the diffraction peak of the (002) plane. This result suggested that the ZnO seed layer had a c-axis preferred orientation. The diffraction peak of the (002) plane was combined with the Debye–Scherrer's equation to calculate the crystalline size of the ZnO seed layer [16]:

$D = (0.9\lambda) / (\beta \text{size} \cos\theta)$ (1)

When the full width at half maximum (FWHM) value of the (002) plane was incorporated into Eq. (1), the crystalline size of the ZnO seed layer was calculated to be 27.6 nm.

The surface morphology and the cross-sectional image of the ZnO seed layer on the p-type Si < 100 > wafer are shown in Fig. 4. We used ZnO gel (i.e., as the precursor) and the spin coating method to prepare the ZnO seed layer. Although the deposited film was annealed at 300°C, the porous state of each particle was distinct at the surface, as shown in Fig. 4(a). The particles were about 30 nm in size, which matched the results obtained using the Debye–Scherrer's equation and the diffraction peak of the (002) plane from Fig. 3. Figure 4(b) shows that the thickness of the ZnO seed layer was about 198 nm, which suggests that the thickness of each coating was approximately 33 nm.

The chemical reactions involved in the fabrication of the ZnO nanorods were divided into metal oxide hydrolysis and dehydration reactions. The chemical reactions are listed below [17, 18]:

$C_6H_{12}N_4 + 6H_2O \rightarrow 6HCHO + 4NH_3$ (2)

$4NH_3 + H_2O \leftrightarrow NH_4^+ + OH^-$ (3)

$$Zn^{2+} + 2OH^- \leftrightarrow Zn(OH)_2 \overset{\Delta}{\leftrightarrow} ZnO_{(s)} + H_2O \quad (4)$$

From these chemical reaction equilibriums we can determine the direction of these chemical equilibrium reactions by controlling the concentrations of the reactants, the synthesis temperature, and the synthesis time. In general, the concentrations of the reactants determine the density of one-dimension ZnO nanorods, while the synthesis temperature and synthesis time affect the morphology, including the diameter, height, and aspect ratio, of the ZnO nanorods.

In this study, the synthesis time was used the parameter to investigate the properties of the ZnO nanorods. The XRD patterns of the ZnO nanorods as a function of synthesis time are shown in Fig. 5. We used the XRD patterns to determine that there was an apparent diffraction peak located at the 2θ value of 34.7°, which corresponded to the (002) plane; two weak diffraction peaks were located at the 2θ values of 31.9° and 36.48°, which corresponded to the (100) and (101) planes, respectively. These results suggested that the ZnO nanorods had a c-axis preferred orientation when the synthesis time increased, and that the synthesis rate along the peak of the (002) plane was more sensitive to the synthesis time compared with the peaks of the (100) and (101) planes. However, the diffraction peaks of the (102) and (110) planes located at the 2θ values of approximately 47.64° and 56.78° were not observed. Figure 5 shows that the diffraction intensity of the (002) plane increased with synthesis time, which suggests that the crystal quality of ZnO nanorods in the (002) plane improved with time. Figure 5 also shows that the diffraction intensities of the (100) and (101) planes decreased with time. The surface and cross-sectional morphologies of the ZnO nanorods as a function of synthesis time are shown in Fig. 6 and Fig. 7, respectively. Figure 6 and Fig. 7 show that as the synthesis time increased, both the height (i.e., length) and the diameter of the ZnO nanorods increased; the aspect ratio (height/diameter) also increased with synthesis time. Because the ZnO nanorods push against each other, they grow perpendicular to the substrate and, therefore, the diffraction intensities of the (100) and (101) planes gradually become weaker.

It is clear that the height, diameter, and aspect ratio, which is defined as the height divided by the diameter, of the ZnO nanorods were closely related to the synthesis time. As Fig. 6 and Fig. 7 show, ZnO nanorods could be observed even when the synthesis time was 10 min. Both the average height and diameter of the ZnO nanorods increased, while the density of ZnO nanorods in a unit area decreased with synthesis time. The height and diameter of the ZnO nanorods were determined from Fig. 6 and Fig. 7. The aspect ratio, which can be used to analyze the relationship between the axial and radial growth of the ZnO nanorods, was calculated using the measured values. Both the height and the diameter of 10 ZnO nanorods were measured to find their average values for synthesis times of 10 min, 20 min, 30 min, and 60 min. When the thickness of the ZnO seed layer was determined to be 200 nm, the average heights of the ZnO nanorods were 42 nm, 130 nm, 335 nm, and 1300 nm, and the average diameters of the ZnO nanorods were 54 nm, 71 nm, 88 nm, and 112 nm, respectively. Correspondingly, the calculated aspect ratios of the ZnO nanorods were 0.78, 1.83, 3.80, and 11.6 when the synthesis time was 10 min, 20 min,

30 min, and 60 min, respectively. A synthesis time of 60 min was optimum for synthesizing ZnO nanorods with a long height, a high aspect ratio, and a well-defined hexagonal prism shape.

As Fig. 6 shows, the diameters and heights of the ZnO nanorods were uniform. Therefore, the relationships shown in Table 1 were used to calculate the radius, height, and aspect ratio of a cube that had been divided into different numbers of cylinders; the results are shown in Table 2. As Fig. 8 shows, when a cylinder (radius $r = a/2$), with side length a and volume $\pi a^3/4$, is divided 4 cylinders ($r = a/4$) or 9 cylinders ($r = a/6$), and the height of each cylinder is a, although the total volumes of the cylinders are equal, the total surface area increases with the number of cylinders. As Table 1 shows, as the radii are $a/2$, $a/4$, and $a/6$, the total surface area are $2\pi\frac{a}{2}\left(\frac{a}{2}+a\right) = 3\pi a^2/2$, $4 \times 2\pi\ a/4\ (a/4+a) = 5\pi a^2/2$, and $9 \times 2\pi\ \frac{a}{6}\left(\frac{a}{6}+a\right) = 7\pi a^2/2$, respectively. Therefore, as the diameter of the ZnO nanorods decreases and the total volume of the nanorods in a unit area is unchanged, the density (i.e., quantity) of the cylinders in a unit area increases, while both the total surface area and the surface area to volume ratio increase. When prepared samples have the same total volumes, the total surface area or the surface area to volume ratio affects the characteristic responses of the ZnO nanostructures and have an effect on their use as optical devices or sensors.

Table 1. The relationship between the radius, height, surface area, volume, and surface area/volume (S/V) ratio of the ZnO nanorods.

radius	$r = \frac{a}{2}$	$r = \frac{a}{4}$	$r = \frac{a}{6}$
height	$h = a$	$h = a$	$h = a$
surface area (S)	$2\pi\frac{a}{2}\left(\frac{a}{2}+a\right)$	$4 \times 2\pi\frac{a}{4}\left(\frac{a}{4}+a\right)$	$9 \times 2\pi\frac{a}{6}\left(\frac{a}{6}+a\right)$
volume (V)	$\pi\left(\frac{a}{2}\right)^2 a$	$4 \times \pi\left(\frac{a}{4}\right)^2 a$	$9 \times \pi\left(\frac{a}{6}\right)^2 a$
S/V	$\frac{6}{a}$	$\frac{10}{a}$	$\frac{14}{a}$

To calculate the density (i.e., quantity) of ZnO nanorods in a unit area, the surface area was divided into squares with an area of 1 μm^2, and Fig. 9 shows 5 sample areas. We randomly sampled 8 squares, calculated the density of ZnO nanorods in each area, and determined the average value. The densities of the ZnO nanorods were 107 μm^{-2}, 94 μm^{-2}, 72 μm^{-2}, and 65 μm^{-2} when the synthesis time was 10 min, 20 min, 30 min, and 60 min, respectively. The measured heights and diameters, as well as the calculated densities, of the ZnO nanorods were used to determine the total surface area (S, nm^2), the total volume (V, nm^3), and the S/V ratio; the results are shown in Table 2 as a function of synthesis time. As the synthesis

time increased from 10 min to 60 min, the total surface area increased from $1.01 \cdot 10^6$ to $3.04 \cdot 10^7$ nm^2, the total volume increased from $1.03 \cdot 10^7$ to $8.32 \cdot 10^8$ nm^3, and the S/V ratio decreased from $9.79 \cdot 10^{-2}$ to $3.65 \cdot 10^{-2}$. These results showed that it was possible to manipulate the height, diameter, and aspect ratio of the ZnO nanorods by controlling the synthesis time.

The main reason for the increases in total surface area and total volume was that the height and diameter of the ZnO nanorods increased with synthesis time, while the density of ZnO nanorods decreased with synthesis time. From the results in Table 2, we know that the growth rate of ZnO nanorods in the vertical-axis direction (i.e., perpendicular to the substrate) was higher than that in the radial-axis direction, even though the density in a unit area decreased with time. ZnO-based materials have a stable crystal plane group, including nonpolar surface groups of {$10\bar{1}0$} and {$21\bar{1}0$}, and a polar surface group of {0001}. In ZnO-based materials, the polar surface is caused by negatively charged oxygen ions and positively charged zinc ions, which form a vertical dipole interaction torque on the c-axis plane [19]. Therefore, the growth rate in the vertical-axis direction is higher than that in the radial-axis direction, which causes the ZnO nanorods to have a c-axis preferred orientation with a high aspect ratio at a long synthesis time.

When the hydrothermal method is used to synthesize ZnO nanomaterials, the polar {0001} plane has a better activity response than the nonpolar {$10\bar{1}0$} and {$21\bar{1}0$)} planes. Therefore, the ZnO materials have a c-axis preferred orientation when forming one-dimensional nanomaterials, such as nanorods or nanowires. There are two factors that cause an increase in the diameter and a decrease in the density of ZnO nanorods. First, during the synthesis process, two adjacent nanorods may combine with each other to form one nanorod, which causes the diameter of the nanorod to increase and the density to decrease. Second, because the growth rate of the nanorods is inconsistent, those with a fast growth rate will remove elements they need, which can cause nanorods that have a slow growth rate to synthesize slower or to stop synthesizing. This causes the density of the nanorods to decrease and the diameter to increase.

Table 2
The density, total surface area (S), total volume (V), and S/V ratio of the ZnO nanorods as a function of synthesis time.

Synthesis time (min)	**10**	**20**	**30**	**60**
Density (quantity per μm^2)	107	94	72	65
Total surface area (S, nm^2)	1.01×10^6	3.10×10^6	7.10×10^6	3.04×10^6
Total volume (V, nm^3)	1.03×10^7	4.84×10^7	1.47×10^8	8.32×10^8
S/V ratio	9.79×10^{-2}	6.40×10^{-2}	4.84×10^{-2}	3.65×10^{-2}

The PL emission spectra were used to analyze the types of defects in the ZnO nanomaterials. The ZnO seed layer and the ZnO nanorods were excited using a laser with an excitation wavelength of 325 nm; the

PL emission spectra were recorded in the range of 350 nm to 650 nm (Fig. 10). The PL emission spectra showed that the ZnO nanorods had one sharp and strong emission peak located at approximately 380 nm, which is the near-band-edge emission; one broad emission band was also observed in the range of 420 ~ 575 nm, which was emitted green light. However, our result of 380 nm differed from the wavelengths reported by Zheng et al., which ranged from 392nm to 397 nm [17], and Lin et al., which was 390 nm [18], but was similar to the 377 nm reported by Li et al [20]. The energy band gap of emission in the range of 420 ~ 575 nm corresponded to the transition between the local level and the near-band-edge. It formed because of defects in the ZnO nanorods; its emission intensity was smaller than that of the emission peak at 380 nm. There are many intrinsic defects that exist in undoped ZnO-based nanomaterials, including oxygen vacancy (V_O, band gap energy (Eg) = 1.62 eV or emission light at ~ 765 nm), interstitial oxygen (O_i, Eg = 2.28 eV or emission light at ~ 544 nm), antisite defects (O_{Zn}, Eg = 2.38 eV or emission light at ~ 521 nm), interstitial zinc (Zn_i, Eg = 2.90 eV or emission light at ~ 428 nm), and zinc vacancy (V_{Zn}, Eg = 3.06 eV or emission light at ~ 405 nm) [18].

It is well accepted that the crystal quality of ZnO nanorods is closely associated with the intensity of the near-band-edge emission, and that the emission intensity in the range of 420 ~ 575 nm is closely related to interstitial oxygen and antisite defects [21]. As Fig. 10 shows, the broad emission intensity of the ZnO seed layer at 420 ~ 575 nm was higher than the intensity for the ZnO nanorods at all synthesis times. This result suggested that the ZnO seed layer had a poor crystal quality and contained many different defects, which could explain the results shown in Fig. 3. Therefore, we can understand that the PL property is dependent on the synthesis time by the fact that the crystal quality of ZnO nanorods can be partly improved with time.

The emission of green light is caused by interstitial oxygen (544 nm) and antisite (521 nm) defects at the local level in the ZnO seed layer and ZnO nanorods (Fig. 10) [18]. The greater the antisite defect is in the ZnO nanorods, the stronger the emission intensity is for green light in the broad emission band of 420 ~ 575 nm. In general, the maximum emission intensity of green light can be used to judge the quality of ZnO nanorods because it indicates the presence of defects. Figure 10 shows that the emission peak of the broad band for the ZnO seed layer is located at 485 nm, while the emission peak of the broad band for the ZnO nanorods shifted from 485 nm to 540 nm as the synthesis time increased from 10 min to 60 min. These results suggested that the ZnO nanorods repaired the interstitial zinc defect faster than they repaired the antisite defect as they were synthesized on the ZnO seed layer. The two defects decreased with synthesis time, which indicated that the crystal quality of the ZnO nanorods was enhanced with time. Thus, ZnO nanorods with a high optical quality may be successfully obtained when the synthesis time is extended

Table 3 shows the emission intensity values of UV (ultraviolet rays) light (I_{UV}), green light (I_G), and the I_G/I_{UV} ratio of the ZnO nanorods as a function of synthesis time. As the synthesis time increased from 10 min to 60 min, the intensity of the I_{UV} value increased from 224 to 742 (a.u.), while the I_G value decreased from 150 to 60.7 and the I_G/I_{UV} ratio decreased from 0.670 to 0.082. These results proved that the defects

in the ZnO nanorods decreased with synthesis time because the crystal quality of the ZnO nanorods improved over time. Li et al. found that an increase in the intensity of UV light was related to the S/V ratio [20]. When the S/V ratio was high, the I_{UV} value was high and the I_G value was low. However, the present research showed a different trend; we found that the I_{UV} of the ZnO nanorods was positively related to the total surface area and the total volume, and was negatively related to the S/V ratio. The increase in the S/V ratio was caused by an increase in the total surface area, which provided more area to absorb the excited light and to emit the emission light. Therefore, we believe that the total surface area enhanced the I_{UV} of the ZnO nanorods.

Vanheusden et al. reported that the near-band-edge emission intensity was closely related to the crystal quality of the prepared ZnO samples [21]. Figure 5 shows that the crystal quality of the ZnO nanorods improved with synthesis time; therefore, the PL properties of the ZnO nanorods were dependent on synthesis time. These results suggested that the decrease in the I_G values and the increases in the I_{UV} values and the I_G/I_{UV} ratio were caused by the enhancement of the crystal quality of the ZnO nanorods. Thus, the total surface area and the crystal quality of ZnO nanorods are important factors that affect the PL properties.

Table 3
The I_{UV} values, I_G values, and the I_G/I_{UV} ratio of ZnO nanorods as a function of synthesis time.

Synthesis time (min)	I_{UV}	I_G	I_G/I_{UV}
10	224	150	0.670
20	287	103	0.359
30	434	74.4	0.171
60	742	60.7	0.082

Figure 11 shows the SEM images of the novel templates at different magnifications, as well as the FIB cross-sectional view. These images showed that the lift-off technology successfully transferred the patterned ZnO seed layer from the sapphire substrate to the p-type Si < 100 > substrate. Figure 11(b) was used to estimate the average particle size and diameter of the top circular plane of the ZnO seed layer, which were determined to be about 32 nm and 365 nm, respectively. The size of the particles were similar to the particle size of the ZnO seed layer that was deposited on the p-type Si < 100 > wafer. The thickness of the ZnO seed layer was obtained from the FIB image after converting its measurement angle, and the measured result was 206 nm, as Fig. 11(c) shows.

The XRD patterns as a function of synthesis time of the ZnO nanoflower arrays are shown in Fig. 12 According to the figure, the diffraction peaks of the (100), (002), (101), (102), and (110) planes corresponded to the peaks located at the 2θ values of 31.9°, 34.6°, 36.48°, 47.64°, and 56.78°, respectively. These results proved that the ZnO nanoflower arrays had an HCP array and a wurtzite

structure. However, there was a large difference between the results shown in Fig. 12 and the results of the ZnO nanorods shown in Fig. 5. The XRD patterns of the ZnO nanorods did not show diffraction peaks of the (102) and (110) planes; the diffraction intensities of the (100) and (101) planes also decreased with synthesis time. In contrast, the diffraction intensities of the ZnO nanoflower arrays in five directions increased with synthesis time. The ZnO nanorods in the nanoflower arrays did not push against each other and, thus, the density did not decrease. This result suggested that that the crystal property can be enhanced with synthesis time. The results also indicated that the ZnO nanoflower arrays did not have a c-axis preferred orientation. The main growth directions of the ZnO nanoflower arrays were not perpendicular to the substrate, but rather spread out like a flower, as shown in Fig. 13.

The surface morphologies of the ZnO nanoflower arrays are shown in Fig. 13 as a function of synthesis time. The figure shows that the growth direction of the ZnO nanorods was not fully perpendicular to the substrate; they grew in the radial direction. Because the growth of the ZnO nanorods followed the protrusion direction of the array-patterned ZnO seed layers, the nanorods had a flower-like structure in which each petal had a single rod shape. The radial ZnO nanorods exhibited a uniform morphology because they had the same diameter and height. This result was attributed to the effects of strong polarization and high synthesis selectivity, which caused the ZnO nanorods to form a ZnO nanoflower in each independent ZnO seed layer. Because the ZnO seed layer was a hexagonal array with a protruding structure in the center of each hexagon, as shown in Fig. 13, the ZnO nanorods grew along the substrate in a vertical direction to form the ZnO nanoflower arrays. The ZnO seed layer arrays were more easily formed using the patterned sapphire template. Thus, this technology played a crucial role in synthesizing ZnO nanorods to form ZnO nanoflower arrays. For the same synthesis time, the height of the ZnO nanoflower arrays was greater than that of the ZnO nanorods. The reason for this observation is that the rod-like ZnO in the ZnO nanoflower arrays grew in the radial direction, which was vertical to the protruding structure in the ZnO seed layer. In addition, the density of the ZnO nanoflower arrays in a unit area was smaller than the density of the ZnO nanorods. Therefore, the main role of $Zn(OH)_2$ in the zinc acetate dehydrate solution was to increase the height of ZnO nanoflower arrays rather than enhance the diameter.

To calculate the density of the ZnO nanoflower arrays in a unit area, the surface area was divided into squares with an area of 1 μm^2, as shown in Fig. 14(a). We randomly sampled eight squares to calculate the density of ZnO nanorods in each area, and calculated the average value. As Fig. 13 sows, the ZnO nanoflower arrays did not fully cover the ZnO seed layer at a synthesis time of 10 min and 20 min. Therefore, the densities were not determined for these times. The densities of the ZnO nanorods were 26 μm^{-2} and 28 μm^{-2} for a synthesis time of 30 min and 60 min, respectively. Figure 14(b) shows the cross-sectional image that was used to calculate the height of the ZnO nanoflower arrays. The heights of the nanoflowers were determined after the thickness of the ZnO seed layer (206 nm) was subtracted. For a synthesis time of 10 min, 20 min, 30 min, and 60 min, the heights of the ZnO nanoflower arrays were determined to be 483 nm, 718 nm, 987 nm, and 1500 nm, and the average diameters were 38 nm, 54 nm,

71 nm, and 90 nm, respectively. Correspondingly, the calculated aspect ratios increased from 12.7, 13.3, 13.9, to 16.7 as the synthesis time increased from 10 min, 20 min, 30 min, and 60 min, respectively.

Figure 15 shows the PL spectra of the ZnO nanorods and ZnO nanoflower arrays as a function of synthesis time. The PL spectra of the ZnO nanoflower arrays had one sharp and strong emission peak located at approximately 380 nm; one broad emission band was also observed in the range of 420 ~ 575 nm. The emission intensities of the 380 nm emission peaks increased with synthesis time, while those of the 420 ~ 575 nm broad emission band decreased with time. Table 4 shows the I_{UV} values, the I_G values, and the I_G/I_{UV} ratio of the ZnO nanoflower arrays as a function of synthesis time. As the synthesis time increased from 10 min to 60 min, the intensity of the I_{UV} value increased from 1156 to 2597 (a.u.), while the I_G value decreased from 337 to 163 and the I_G/I_{UV} ratio decreased from 0.291 to 0.062. For the same synthesis time, the maximum emission intensities of the 380 nm emission peak and the broad emission band of the ZnO nanoflower arrays were larger than those of the ZnO nanorods. These results indicated that the I_{UV} and I_G values of the ZnO nanoflower arrays were larger than those of the ZnO nanorods and, thus, the I_G/I_{UV} ratios of the ZnO nanoflower arrays were smaller than those of the ZnO nanorods. These results also proved that for the same synthesis time, there were more defects in the ZnO nanoflower arrays, as indicated by the I_G value, than in the ZnO nanorods. In addition, the I_{UV} and I_G values were stronger than those of the ZnO nanorods. A comparison of Fig. 6 and Fig. 13 showed that the top surface of the ZnO nanorods was the main area that received the excitation laser light and emitted the PL spectra; the sides of the ZnO nanorods received almost no excitation laser light and emitted no UV or visible light. However, laser light can irradiate all surfaces of the ZnO nanoflower arrays. Thus, we proved that the ZnO nanoflower arrays have better light characteristics than the ZnO nanorods because they have more area to receive light and emit the PL spectra.

Table 4
The I_{UV} values, I_G values, and the I_G/I_{UV} ratio of ZnO nanoflower arrays as a function of synthesis time.

Synthesis time (min)	I_{UV}	I_G	I_G/I_{UV}
10	1156	337	0.291
20	1804	263	0.145
30	2161	258	0.119
60	2597	163	0.062

Conclusions

As the synthesis time increased, the XRD patterns showed that the ZnO nanorods had a c-axis preferred orientation, and that their main growth rate was along the (002) plane. The ZnO nanoflower arrays had 5 diffraction peaks at the (100), (002), (101), (102), and (110) planes, which suggested that the direction of

their growth was not fully perpendicular to the substrate. For both the ZnO nanorods and the ZnO nanoflower arrays, the average height, average diameter, and aspect ratio increased with time. In addition, the I_{UV} values and the I_G/I_{UV} ratio increased with synthesis time, while the I_G values decreased with time. The most important result of this study was that the I_{UV} values of the ZnO nanoflower arrays were stronger than the I_{UV} values of the ZnO nanorods. The results in this study also proved that when the hydrothermal method was used with a patterned sapphire template and the lift-off technique to synthesize ZnO nanoflower arrays, the PL properties of the ZnO nanorods were enhanced.

Declarations

Acknowledgments: This work was supported by projects under Nos. MOST 109-2221-E-390-023, MOST 110-2622-E-390-002, and MOST 110-2221-E-390-020.

References

1. Crisler DF, Cupal JJ, Moore AR (1956) Dielectric, piezoelectric and electromechanical coupling constants of zinc oxide crystals. Proc IEEE 56:225–226
2. Wang FH, Chen KN, Hsu CM et al (2016) Investigation of the Properties of the Nano-Scale GZO Thin Films on Glass and Flexible. Polyimide Substrates Nanomaterials 6:88
3. Saadeldin MM, Desouky OA, Ibrahim M et al (2018) Investigation of structural and electrical properties of ZnO varistor samples doped with different additives. NRIAG J Astron Geophys 7:201–207
4. Tsukazaki A, Kubota M, Ohtomo A, et al. Blue Light-Emitting Diode Based on ZnO. Jpn J Appl Phys. 2005, 44: L443.
5. Manekkathodi A, Wu YJ, Chu LW et al (2013) Integrated optical waveguide and photodetector arrays based on comb-like ZnO structures. Nanoscale 5:12185–12191
6. Nguyen VH, Resende J, Papanastasiou DT et al (2019) Low-cost fabrication of flexible transparent electrodes based on Al doped ZnO and silver nanowire nanocomposites: impact of the network density. Nanoscale 11:12097–12107
7. Ho RVKC. Zinc oxide based dye-sensitized solar cells: A review, Renew Sustain Energy Rev. 2017, 70: 920–935.
8. Aljaafari A, Ahmed F, Awada C et al (2020) Flower-Like ZnO Nanorods Synthesized by Microwave-Assisted One-Pot Method for Detecting Reducing Gases: Structural Properties and Sensing Reversibility. Front Chem 8:456
9. Bhati VS, Kumar MHM (2020) Enhanced sensing performance of ZnO nanostructures-based gas sensors: A review. Energy Rept 6:46–62
10. Karthik TVK, Lugo VR, Hernandez AG et al (2019) Low temperature facile synthesis of ZnO nuts and needle like microstructures. Mater Lett 246:56–59

11. Zhang J, Sun LD, Yin JL et al (2002) Control of ZnO Morphology via a Simple Solution Route. Chem Mater 14:4172–4177
12. Chen YC, Cheng HY, Yang CF et al. Investigate the Optimal Parameters in Hydrothermal Method for the Synthesis of ZnO Nanorods. J. Nanomaterials, 2014, **2014**: 430164
13. Zhang H, Yang D, Li DS et al (2005) Controllable Growth of ZnO Microcrystals by a Capping-Molecule-Assisted Hydrothermal Process. Cryst Growth Des 5:547–550
14. Wang H, Xie J, Yan K et al (2011) Growth Mechanism of Different Morphologies of ZnO Crystals Prepared by Hydrothermal Method. J Mater Sci Technol 27:153–158
15. Katiyar A, Kumar N, Shukla RK et al (2020) Substrate free ultrasonic–assisted hydrothermal growth of ZnO nanoflowers at low temperature. SN Appl Sci 2:1386
16. Chen CC, Wang FH, Chang SC et al (2018) Using Oxygen Plasma Pretreatment to Enhance the Properties of F-Doped ZnO Films Prepared on Polyimide Substrates. Materials 11:1501
17. Zheng WJ, Tzou WC, Shen JR et al (2019) Effect of the Concentration of Eu^{3+} Ions on Crystalline and Optical Properties of ZnO Nanowire. Sens Mater 31:447–455
18. Lin B, Fu Z, Jia Y et al (2001) Defect photoluminescence of undoping ZnO films and its dependence on annealing conditions. J Electrochem Soc 148:G110–G113
19. Li QW, Bian JM, Sun JC et al (2010) Controllable growth of well-aligned ZnO nanorod arrays by low-temperature wet chemical bath deposition method. Appl Sur Sci 256:1698–1702
20. Ahsanulhaq Q, Umar A, Hahn YB (2007) Growth of aligned ZnI nanorods and nanopencils on ZnO/Si in aqueous solution: growth mechanism and structural and optical properties. Nanotechnology 18:115603
21. Vanheusden K, Seager CH, Warren WL et al (1996) Correlation between photoluminescence and oxygen vacancies in ZnO phosphors. Appl Phys Lett 68:403

Figures

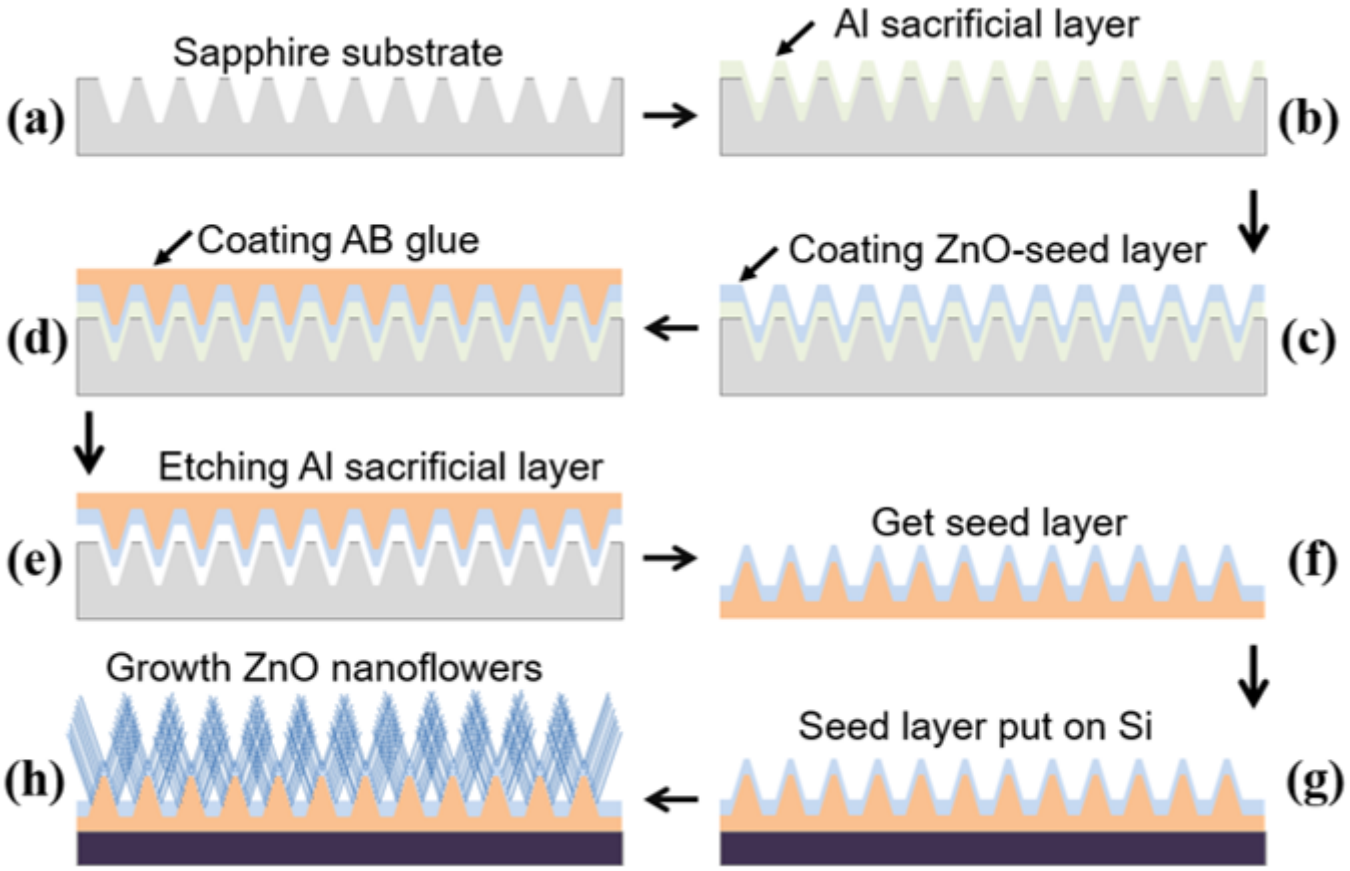

Figure 1

Schematic diagram of the fabrication of ZnO nanoflower arrays.

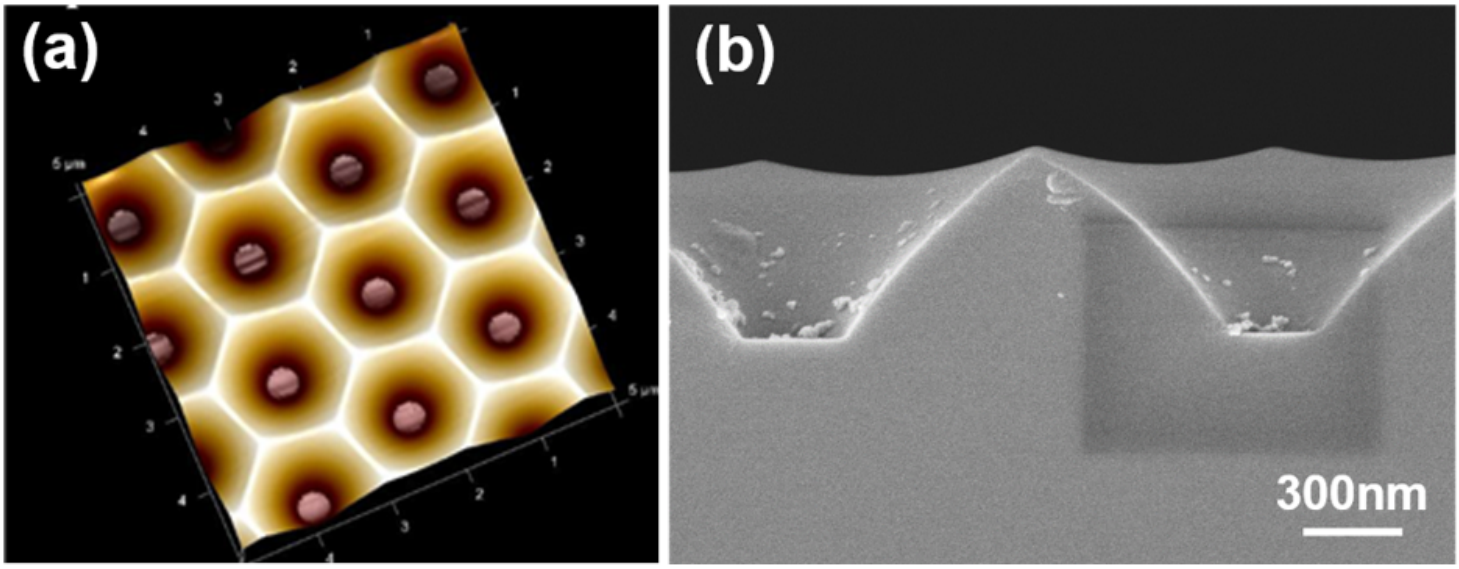

Figure 2

(a) Schematic diagram and (b) cross-sectional view of the 2-inch sapphire substrate.

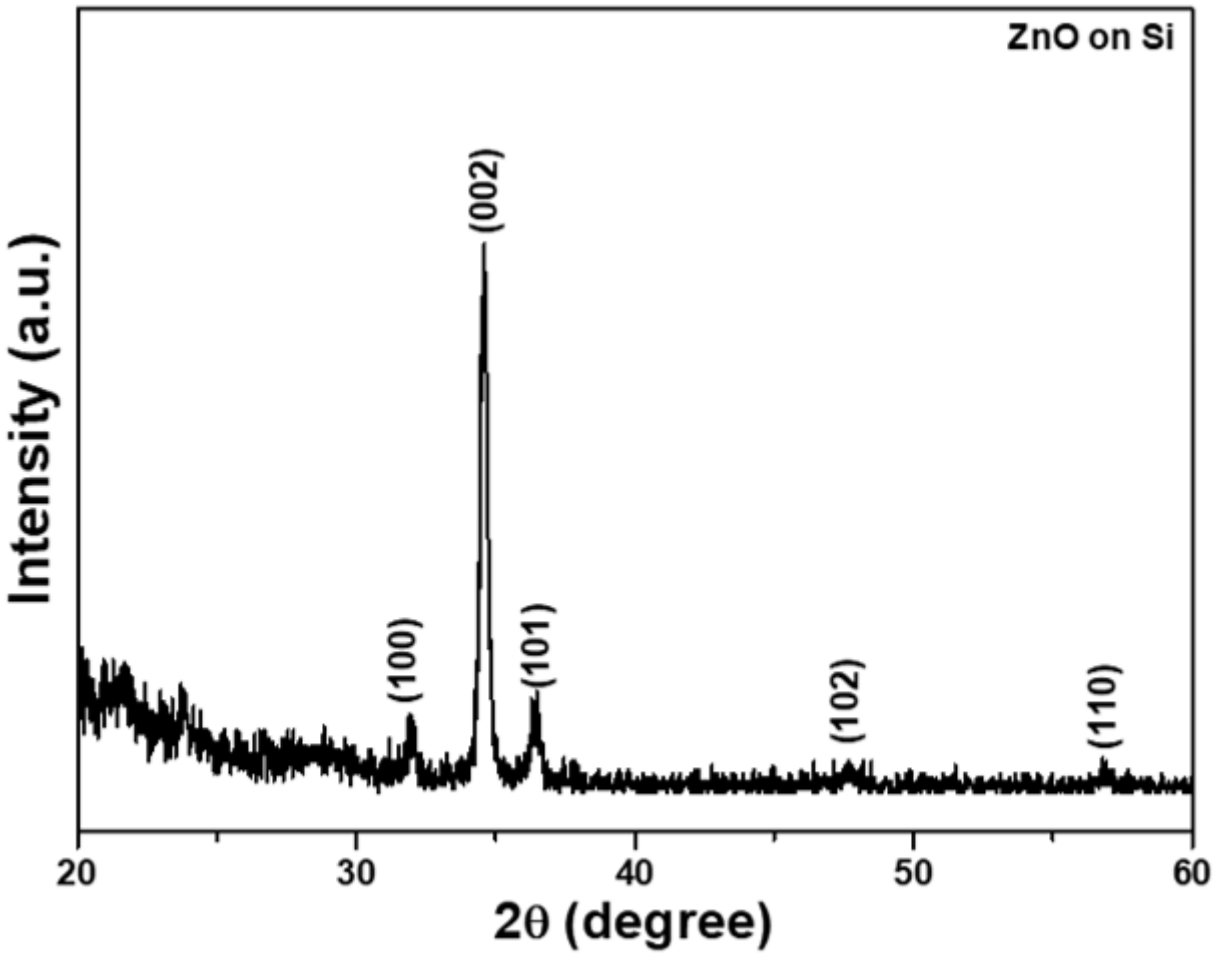

Figure 3

The XRD pattern of the ZnO seed layer on the p-type Si substrate.

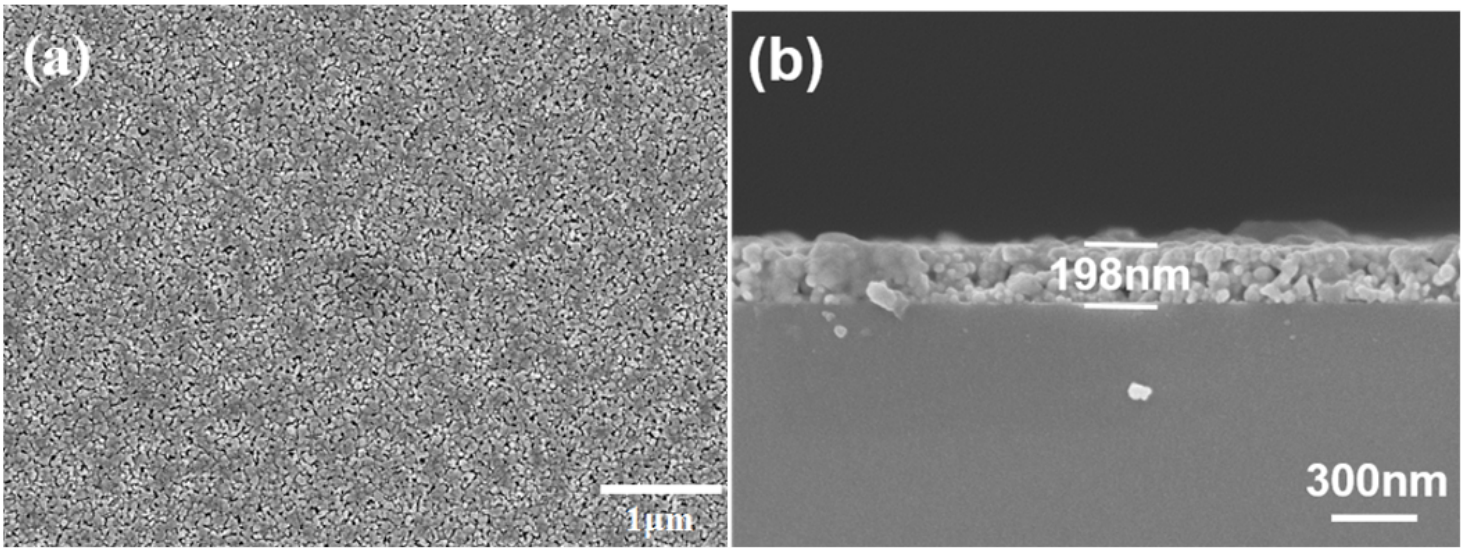

Figure 4

(a) Surface morphology and (b) cross-sectional image of ZnO-seed layer.

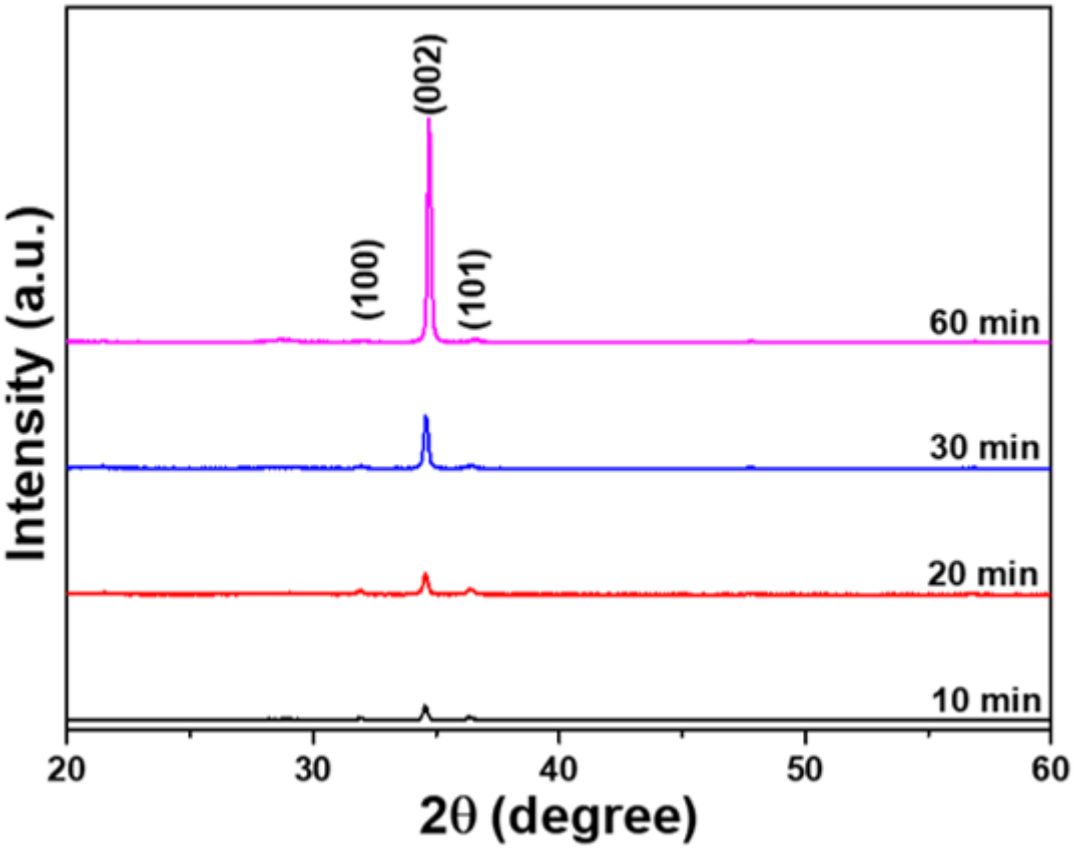

Figure 5

The XRD patterns of the ZnO nanorods as a function of synthesis time.

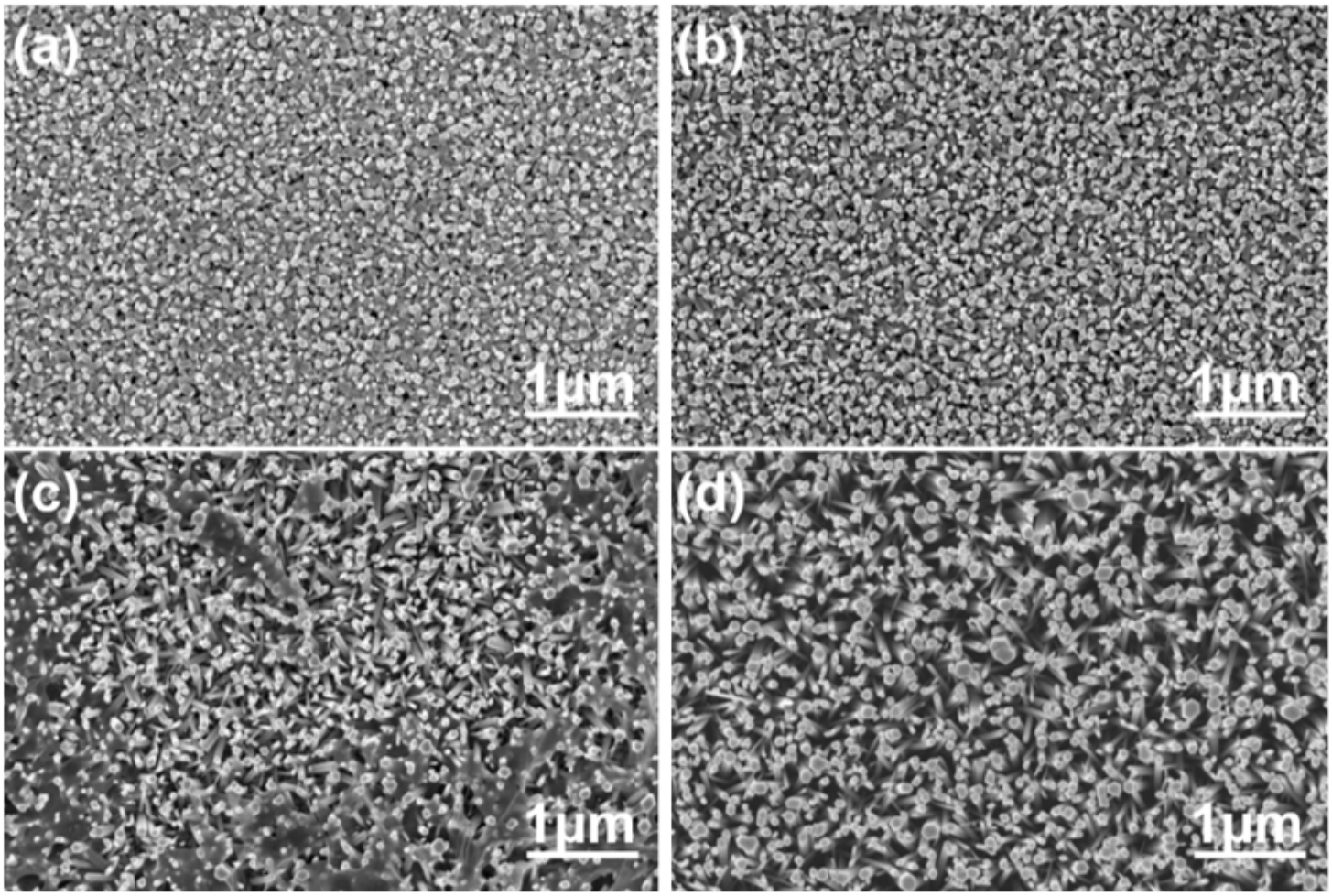

Figure 6

SEM images of the surface morphologies of ZnO nanorods as a function of synthesis time: (a) 10 min, (b) 20 min, (c) 30 min, and (d) 60 min.

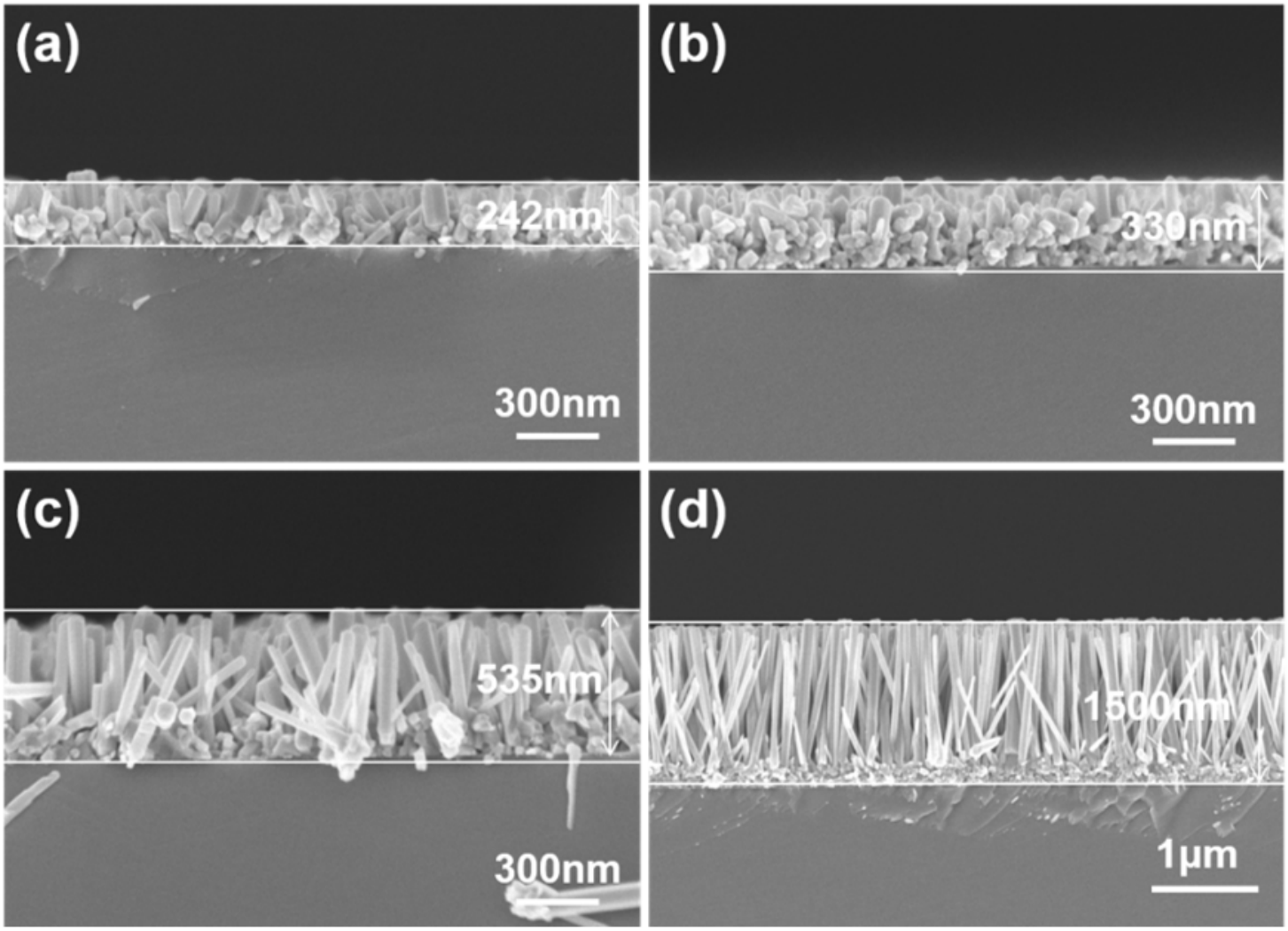

Figure 7

Cross-sectional morphologies of ZnO nanorods as a function of synthesis time, (a) 10 min, (b) 20 min, (c) 30 min, and (d) 60 min.

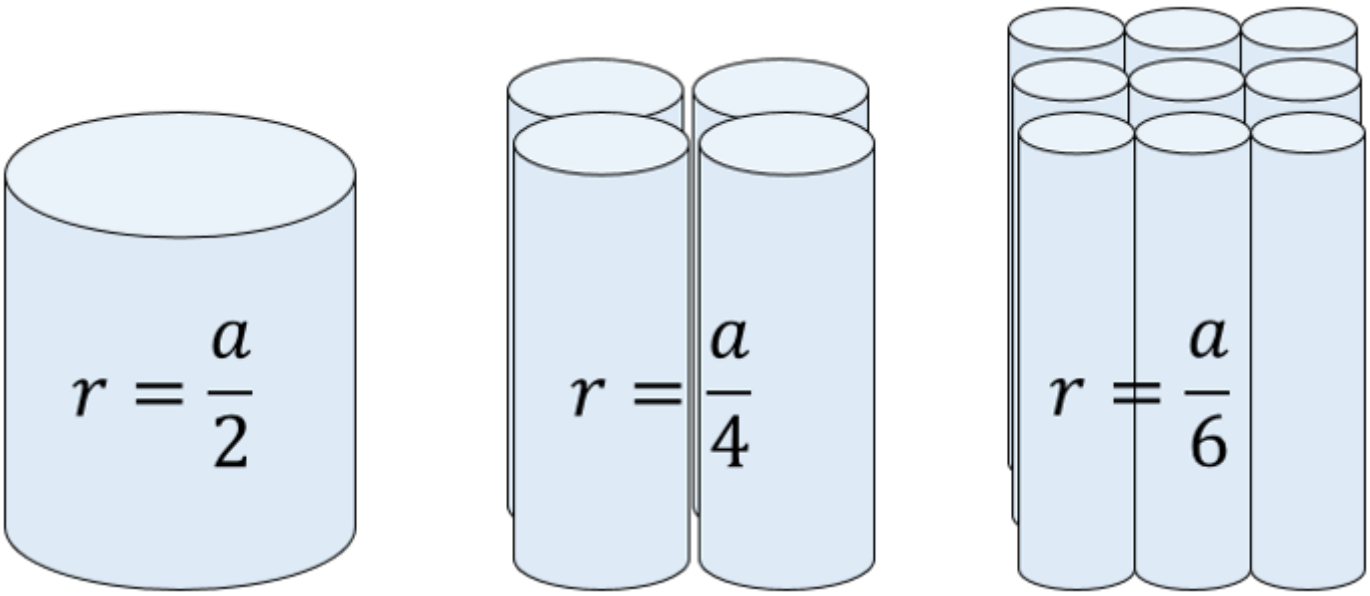

Figure 8

Cylinders with different diameters.

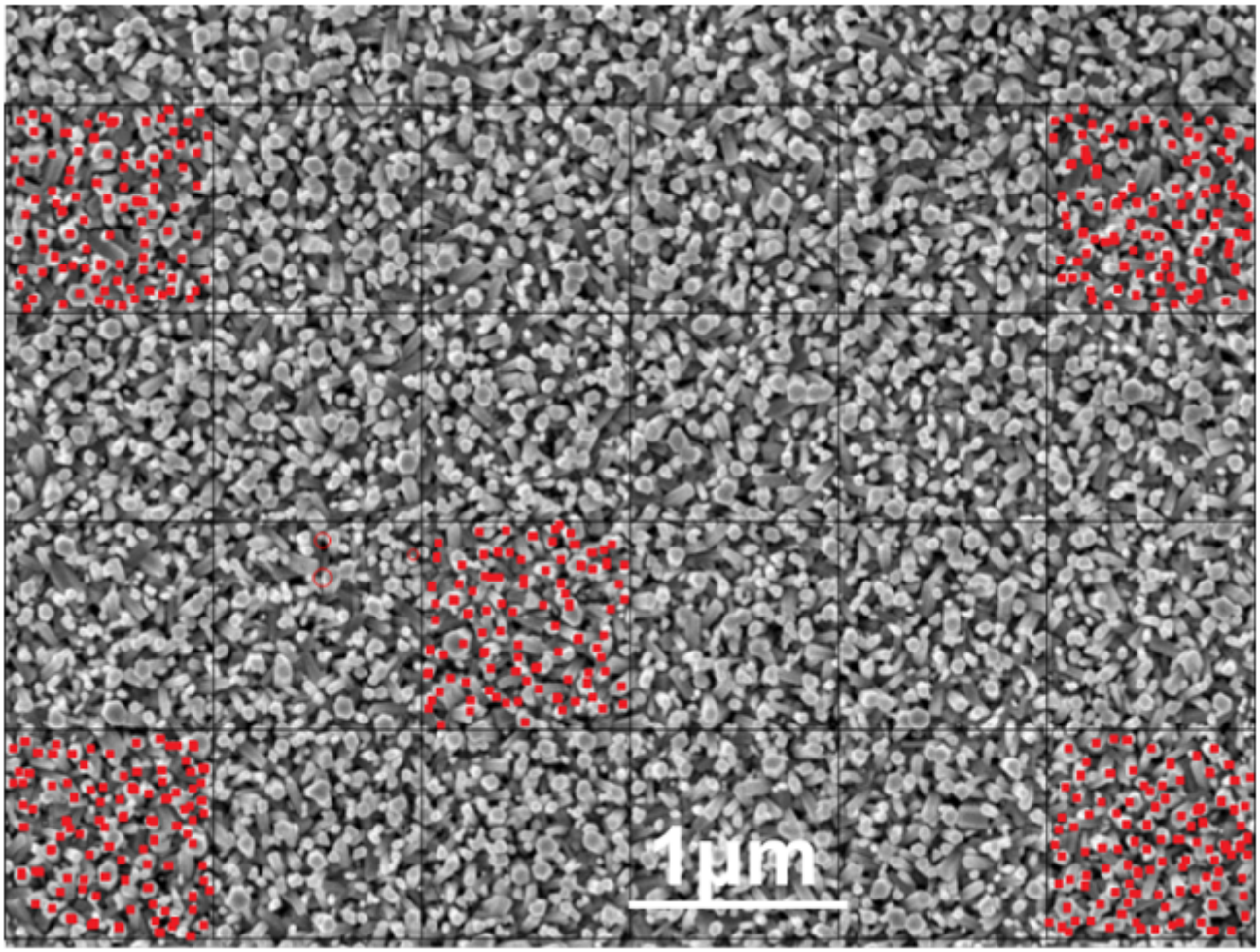

Figure 9

The surface morphology was used to calculate the density of the ZnO nanorods.

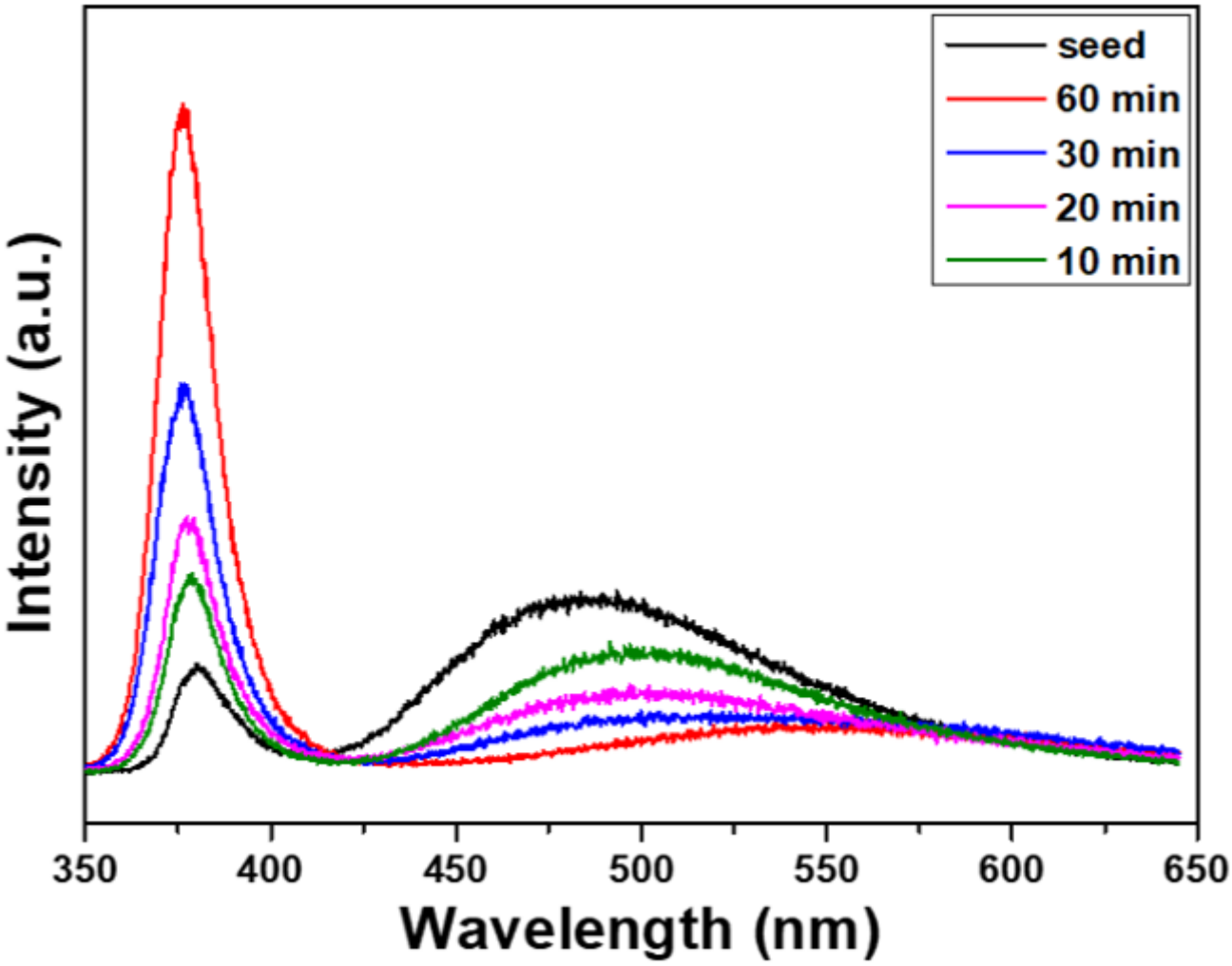

Figure 10

The PL emission spectra of the ZnO nanorods as a function of synthesis time.

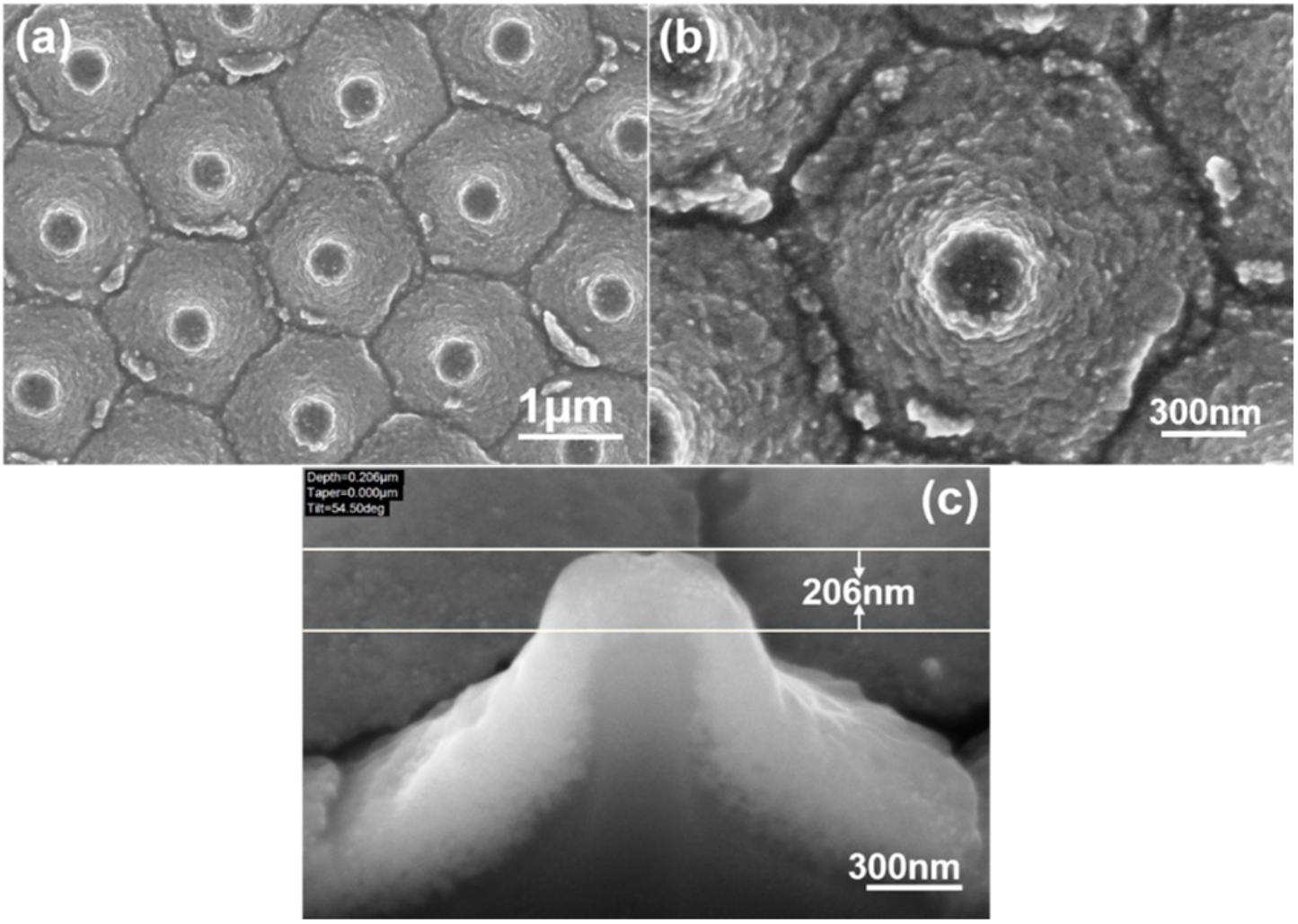

Figure 11

SEM images of the novel templates at (a) a low magnification and (b) a high magnification on the surface observations; and (c) the FIB cross-sectional view of the template.

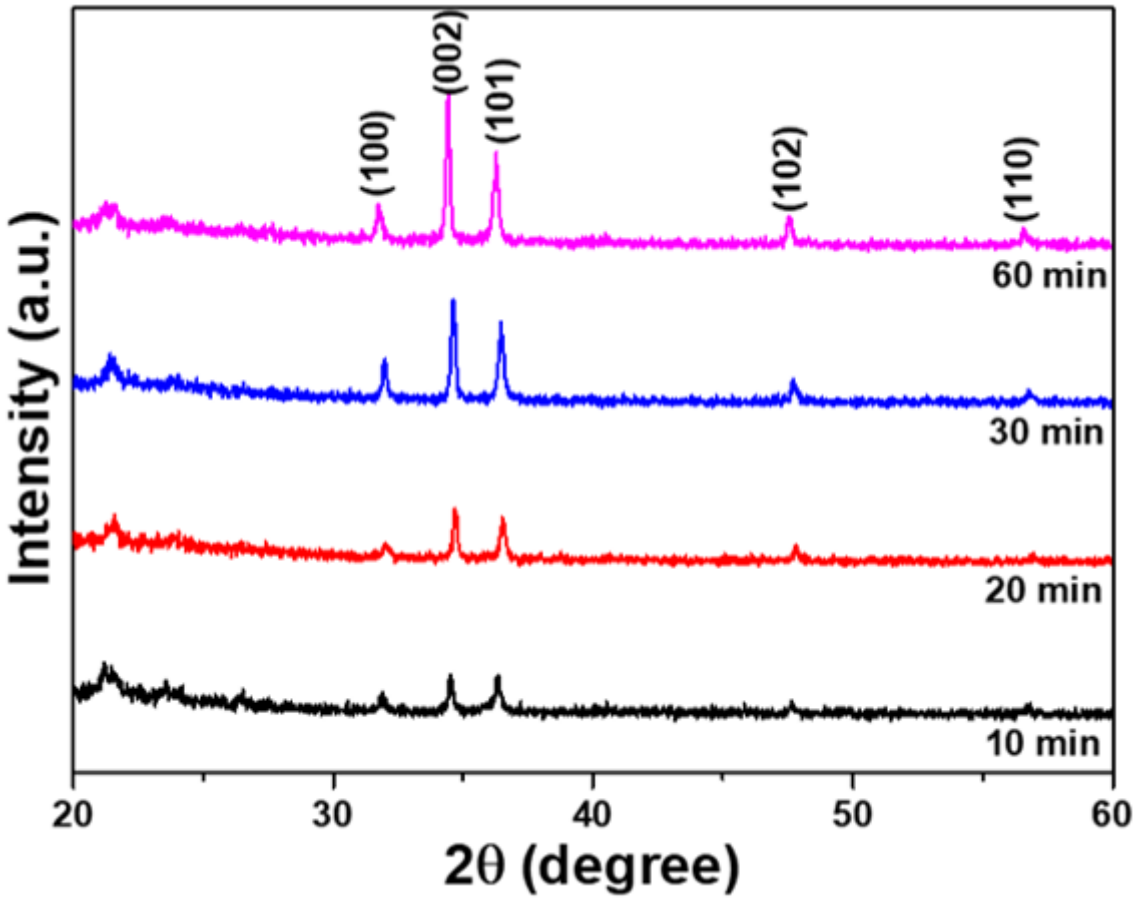

Figure 12

The XRD patterns of ZnO nanoflower arrays as a function of synthesis time.

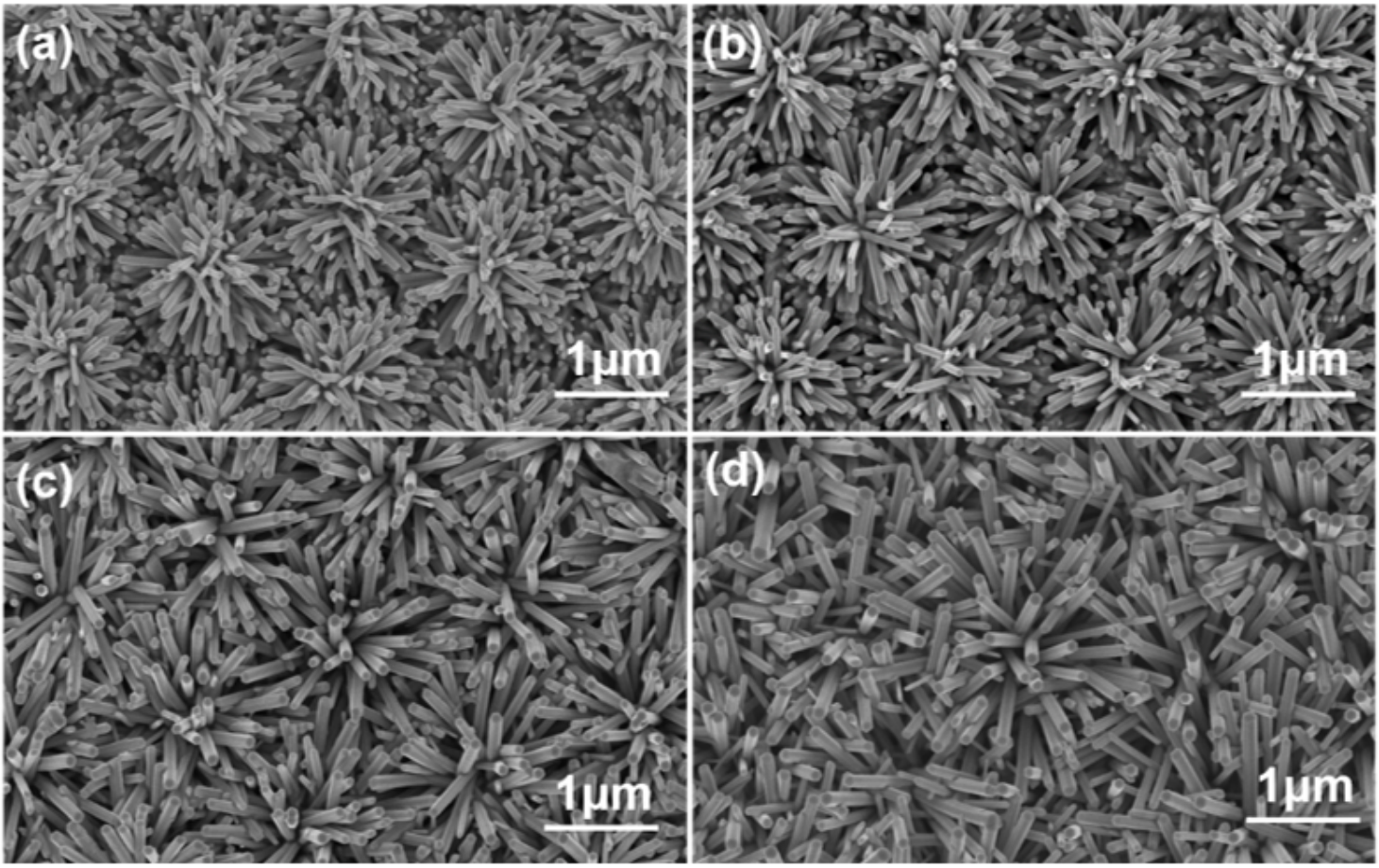

Figure 13

Surface morphologies of ZnO nanoflower arrays as a function of synthesis time: (a) 10 min, (b) 20 min, (c) 30 min, and (d) 60 min.

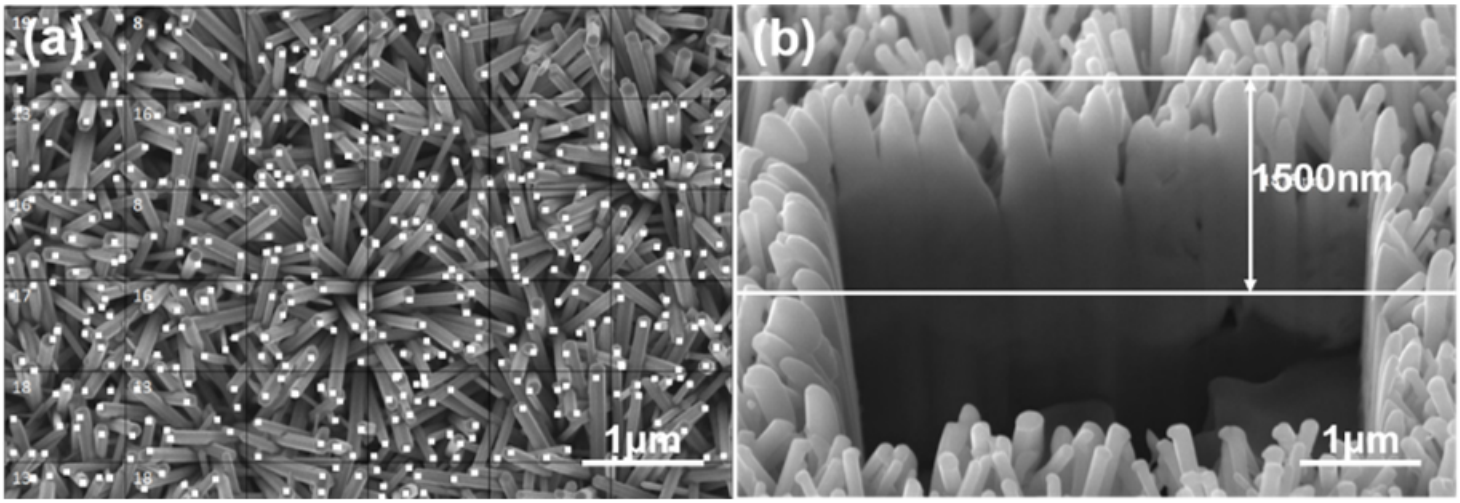

Figure 14

(a) The surface morphology was used to calculate the density of the ZnO nanoflower arrays. (b) A cross-sectional image was used to calculate the height of the ZnO nanoflower arrays.

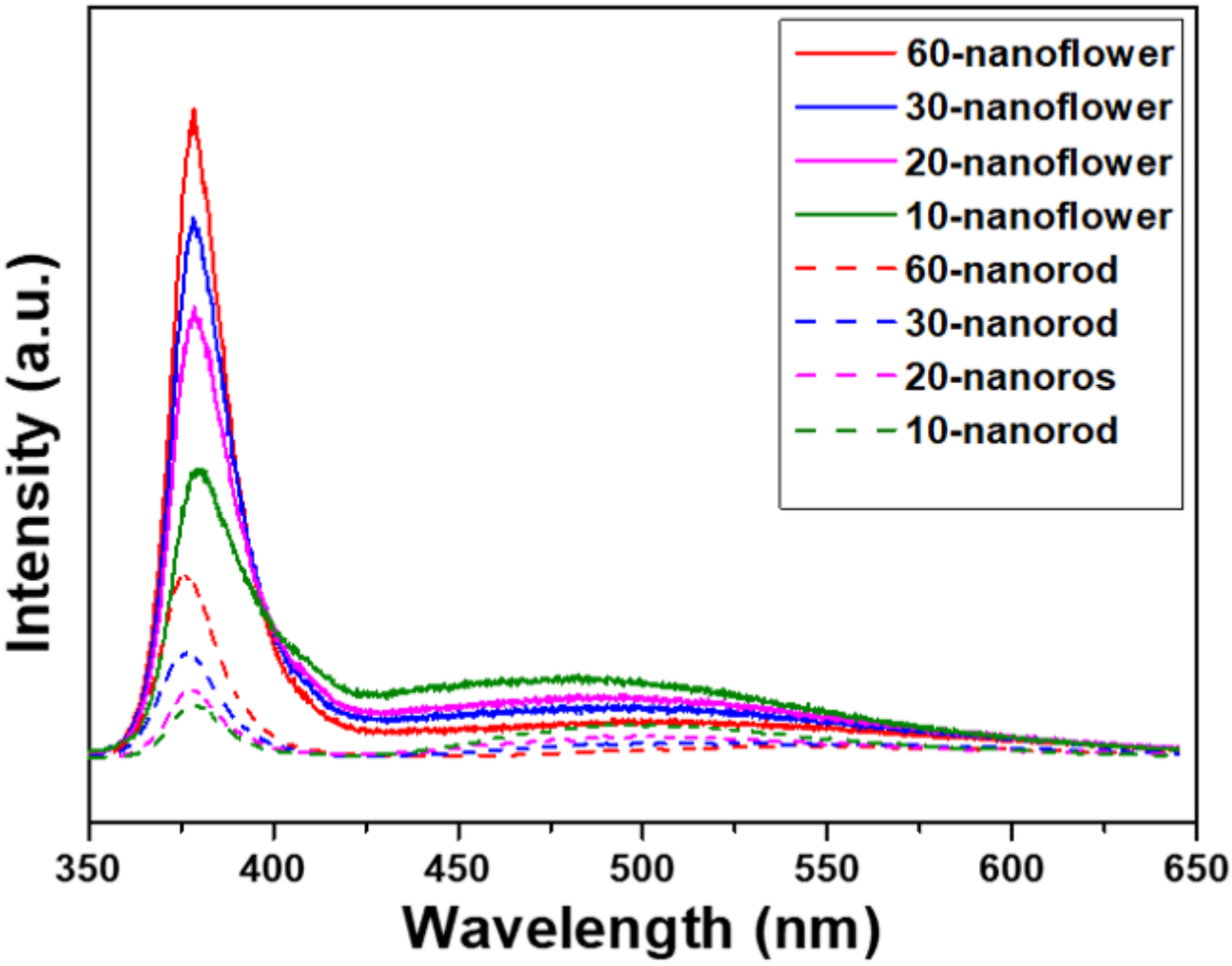

Figure 15

The PL emission spectra of the ZnO nanorods and ZnO nanoflower arrays as a function of synthesis time.